Int J Solids Structures Vol 18, No 3, pp 229–234, 1982
Printed in Great Britain

0020-7683/82/030229-06$03.00/0
Pergamon Press Ltd

PENETRATION EXPERIMENTS FOR NORMAL IMPACT INTO GEOLOGICAL TARGETS†

M. J. FORRESTAL and D. E. GRADY
Sandia National Laboratories, Albuquerque, NM 87185, U S.A

(*Received* 16 *March* 1981; *in revised form* 18 *May* 1981)

Abstract—A laboratory procedure, which determines resultant forces on penetrators for normal impact into geological targets, is explored. Seven experiments were conducted with conical-nosed penetrators impacted by foundry core targets (a simulated soft sandstone). Rigid body velocity of the penetrators was measured with laser interferometry and maximum decelerations and resultant forces were obtained from these data. It is concluded that this laboratory procedure can help evaluate the validity or the weaknesses of theoretical models

INTRODUCTION

Penetration into geological targets has been studied for a wide range of applications, many of which are discussed in [1]. Studies in this field usually focus on the prediction and measurement of penetration depth or deceleration history. Predictive techniques for these quantities are: (1) empirical equations for final penetration depth based on test data[2], (2) models which approximate the target response by 1-dimensional motion using cavity expansion methods[3, 4], and (3) detailed 2-dimensional wave code solutions[5]. All these predictive procedures contain approximations and suffer from inadequate constitutive data for the strain rates that occur during a penetration event.

In [6] the initial motion of ogival-nosed solid steel penetrators with length 50.8 mm (2.00 in.) and diameter 12.7 mm (0.50 in.) was examined analytically and experimentally. Two experiments were conducted in which stationary penetrators were impacted with sandstone targets accelerated to a steady velocity by a light-gas gun. Back surface particle velocity was measured with laser interferometry and the pressure magnitude of the initial nosetip loading was determined with the aid of an asymptotic theory for wave motion in the penetrator. An important conclusion from this study was that the initial transient loading does not produce jumps in the velocity response. This study is, however, limited to the very early time response or the time corresponding to 4.5 mm (0.18 in.) of penetration depth and the maximum force on the penetrator nose is not reached during this time.

In the present paper, a procedure is devised to obtain velocity measurements for sufficient time to determine the maximum force on the penetrator nose. Maximum forces determined from seven experiments with conical-nosed penetrators impacted by foundry core targets are compared with predictions from a recently derived cavity expansion theory[3]. The limitations of predictive methods are discussed, and it is suggested that laboratory penetration experiments, such as these, can help evaluate the validity and the weakness of theoretical models.

REVERSE BALLISTICS EXPERIMENTS

Seven experiments were conducted in which conical-nosed steel penetrators were impacted with foundry core targets. Foundry core is a manufactured material which simulates very soft sandstone or cemented sand and can be produced with negligible sample-to-sample variation. A 0.10 m (3.94 in.) diameter light-gas gun, similar to that described by Fowles[7], was used to accelerate the target to a steady velocity after which the target impacted the conical-nosed penetrators at normal incidence. Geometry of the steel penetrators and target impact velocities are given in Table 1 and a schematic of the experimental arrangement is shown in Fig. 1. A more complete description of the experimental details is provided in [6, 8].

Displacement interferometry was used to measure axial displacement of the center of the penetrator back surface for a time of about 1.5 nose lengths of penetration. With this technique the back surface of the penetrator is used as one of two mirrors in a Michelson displacement interferometer. As the back surface of the penetrator moves, the interferometer provides a

†This work was supported by the U.S Dept. of Energy and the U.S. Army, Pershing II Project Manager's Office

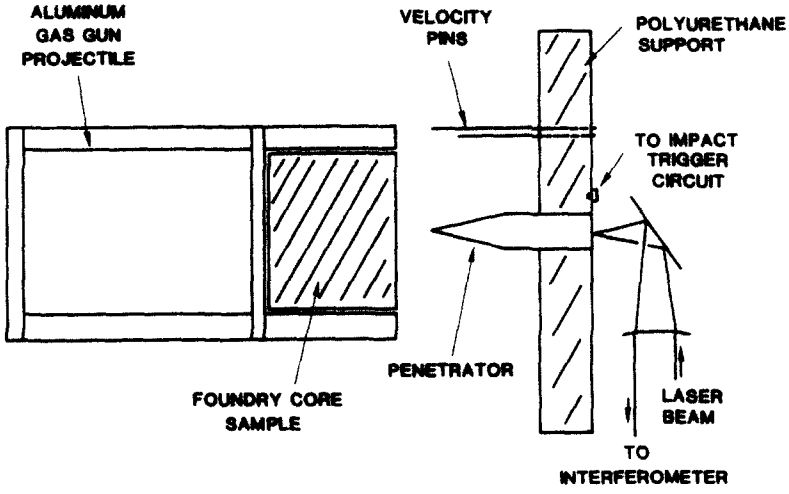

Fig. 1. Schematic of the reverse ballistics experiments

fringe signal directly proportional to the surface displacement. For the He–Ne laser used, each fringe corresponds to 0.314 μm displacement. Continuous displacement-time recording during the full time of interest was not practical due to the large number of fringes occurring and 4 or 5 oscilloscopes were used to sample discrete intervals of time ($\sim 1\ \mu$s) out of approximately 100 μs. In these intervals, 20–30 displacement fringes were measured and velocity was determined by differentiating the data with the technique described in [9]. Based on the instrumentation capability an error of less than two percent was estimated in the velocity data.

Velocity-time data for Test 5 described in Table 1 is shown in Fig. 2 (Complete documentation of the experimental results is available in [8].) The first full nose length of penetration occurs at $t = 61\ \mu$s and after this time the penetrator velocity is nearly linear with time over the interval of measurement. The maximum acceleration data presented in Table 1 were obtained from a straight line fitted through these velocity-time data as shown in Fig. 2. Tests 5–7 indicate excellent repeatability.

TARGET MATERIAL DESCRIPTION

Foundry core was selected for the target material because it has properties similar to very soft sandstone or a cemented sand. This material can be made conveniently for the different sample sizes required for material properties measurements and reverse ballistics tests. The foundry core samples were made at the Sandia foundry with the same process as that used for making molds for metal castings. This material† is primarily silica sand and is combined with sufficient binder ingredients such that when oven fired, a low density sand brick results. The density of the samples was 1.46 Mg/m^3 with variations within one percent among samples.

For input to a recently derived theory[3], the hydrostat and shear failure–pressure relation‡ were obtained from triaxial tests. These data§ were obtained from the procedures described in [10–12] and are presented in Figs. 3 and 4. Data are presented in Fig. 3 from four experiments measuring hydrostats in which different rates of loading (time to peak pressure) are employed. Since the reverse ballistics experiments are monitored over $\sim 100\ \mu$s, data from the experiments with the two shortest rise times are used for the analysis presented in the next section. In addition, a straight line was fit to these data over $0 < p < 50$ MPa with the least squares method and the slope of this line is $K = 300$ MPa. The maximum computed pressures for the experiments range from 18 to 54 MPa.

†Complete material composition is given in [8].

‡The hydrostat is the relationship between pressure p and volume change per original volume η. Shear failure is the difference of the principal stresses at failure and designated as τ. These notations are those used in [3].

§These experiments were conducted by J. Q Ehrgott of the Waterways Experiment Station, Vicksburg, MS 39180.

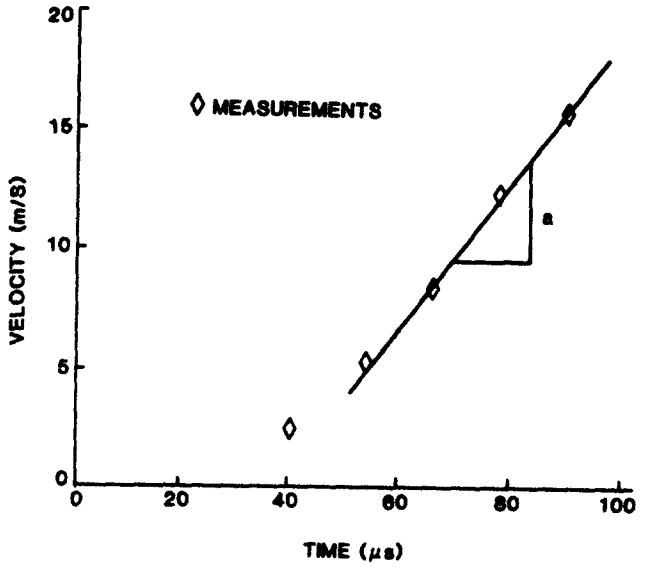

Fig. 2 Velocity-time history of the penetrator for test 5.

Table 1. Summary of measured and predicted results. All penetrators have afterbody length 25.4 mm (1.0 in.) and diameter 12.7 mm (0.50 in.). Target properties are $K = 300$ MPa, $\mu = 0.90$ and $\rho_0 = 1.46$ Mg/m^3

Test Number	Nose Length (mm)	Target Velocity (m/s)	Measured Acceleration (km/s^2)	Predicted Acceleration with f=0 (km/s^2)	Predicted Acceleration with f=0.08 (km/s^2)
1	25.4	240	145	113	149
2	25.4	403	323	221	292
3	25.4	557	392	331	437
4	19.0	239	236	180	223
5	19.0	310	303	233	289
6	19.0	312	290	234	290
7	19.0	313	286	235	291

Shear failure data at various confining pressures were obtained from static triaxial tests† and these data are presented in Fig. 4. As indicated in [10] the foundary core material did not have a distinct yield, but exhibited some hardening for axial strains up to $\epsilon_x = 0.15$. For this reason Hadala and Ehrott[10] suggest shear failure–pressure relations corresponding to the principal stress differences τ at axial strains of $\epsilon_x = 0.10$ and 0.15. For $\epsilon_x = 0.10$ the slope of the τ–p line is $\mu = 0.75$ and for $\epsilon_x = 0.15$, the slope is $\mu = 0.90$. An estimate for penetration resistance sensitivity to μ is provided in Fig. 5 which is discussed in the next section.

ANALYTICAL MODEL FOR NOSE FORCES

A model to estimate forces on conical-nosed penetrators for normal impact into targets described with linear hydrostats and linear shear failure–pressure relations was recently developed[3]. For this analysis, the cylindrical cavity expansion approximation was employed which idealizes the target as thin independent layers normal to the penetration direction and

†The authors did not have access to a test apparatus which could provide shear failure at various strain rates. It should, however, be pointed out that experiments concerned with shear failure at confining pressures with various strain rates have been reported[13].

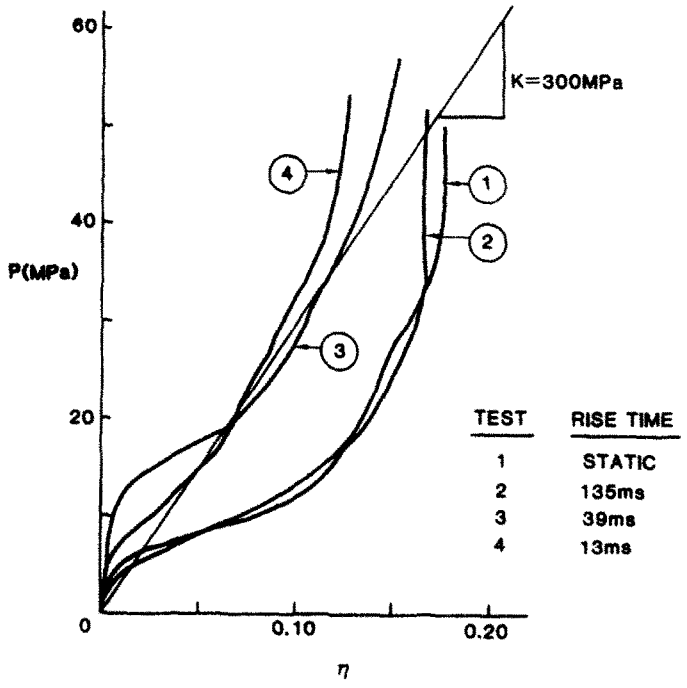

Fig. 3 Hydrostat data from [11] and the linear fit

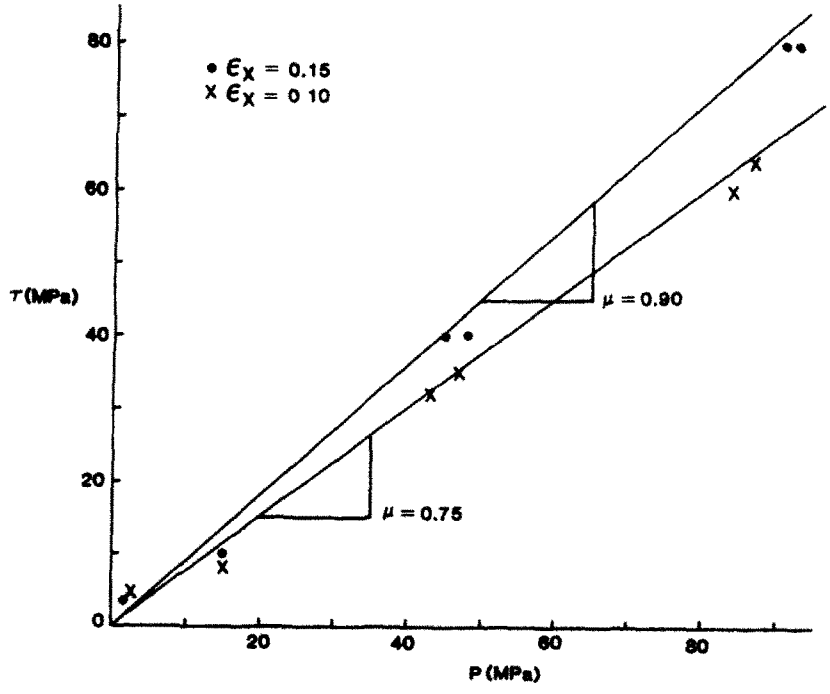

Fig. 4. Linear shear failure relations and data from [10]

permits 1-dimensional wave propagation calculations in the radial coordinate. This model predicts spatially uniform radial stress σ_r on a conical penetrator nose, and generalized curves for radial stress are presented in Fig. 5 for two slopes of the shear failure–pressure relationship (see Fig. 4). Other definitions used in Fig. 5 are: K is the slope of the hydrostat (see Fig. 3), V_t is the target impact velocity, θ is the half-conical angle of the nose, and ρ_0 is the original target

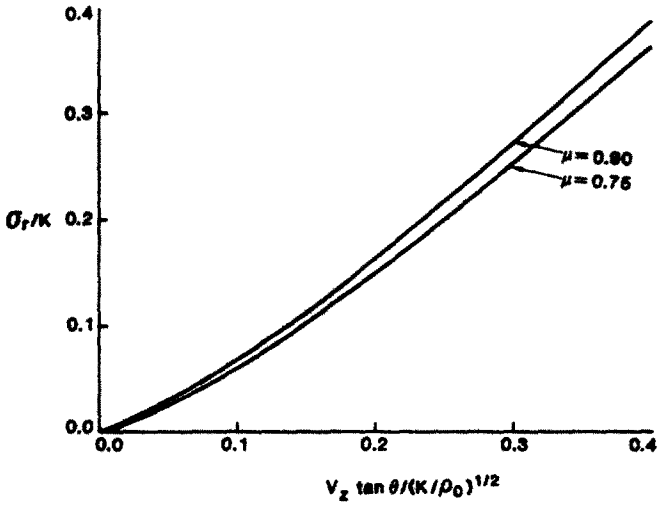

Fig. 5. Radial stress component on the conical nose for $\mu = 0.90$ and 0.75.

density. The resultant resisting force on the nose and rigid body acceleration are given by

$$F_z = \pi \bar{r}^2 \sigma_r; \; a = F_z/m \tag{1}$$

where $\bar{r}$ is the radius of the cylindrical afterbody, m is the total mass of the penetrator, and σ_r is given in Fig. 5.

Another source of resistance to penetration is the tangential interface friction between the penetrator nose and foundry core target. A posttest photograph of the penetrator used in Test 2 is shown in Fig. 6. Prior to impact by the foundry core target, the entire penetrator surface looked like the cylindrical region just aft of the conical nose. Evidence of friction and wear is apparent from this posttest photograph. As discussed by Longcope and Grady[6], the equations for resultant force and acceleration with the inclusion of sliding friction are

$$F_z = \pi \bar{r}^2 \sigma_r (1 + f/\tan\theta); \; a = F_z/m \tag{2}$$

where f is the coefficient of sliding interface friction. Friction phenomena at very high speed is discussed by Bowden and Tablor[14] and for the velocity regime of this study, data in [14, 15] suggests $f = 0.08$.

SUMMARY OF RESULTS AND DISCUSSION

A summary of the experimental and predicted results are given in Table 1. The agreement between predicted acceleration with $f = 0.08$ (friction coefficient taken from [14]) and the measurements is extremely close in view of the many approximations used in the theoretical model. Major assumptions in the model are: (1) the cylindrical cavity expansion approximation which considers the target as independent layers normal to the penetration direction and assumes only radial target motion, (2) a constitutive target description that contains minimum detail; a linear hydrostat and a linear shear failure–pressure relation, and (3) a sliding friction coefficient obtained from experimental situations very different from penetration events. Even with the simplifying assumptions used in [3], it is a major problem to obtain target material property data at the rates that occur during a penetration event. In this paper, hydrostat data are employed for tests performed over 10–40 ms, whereas measurements of penetrator velocity for the reverse ballistics tests are taken over 100 μm. Furthermore, the shear failure data were obtained from static tests. Clearly, mathematical models are valuable and enable one to project to situations not attainable with full-scale tests, but the accuracy of any model which predicts forces on penetrators is dependent on the quality of the target material data. The repeatability of the measurements from Tests 5–7, however, clearly indicates that this laboratory procedure can be successfully used to evaluate the validity or the weakness of theoretical models for other target materials, penetrator geometries and impact velocity regimes.

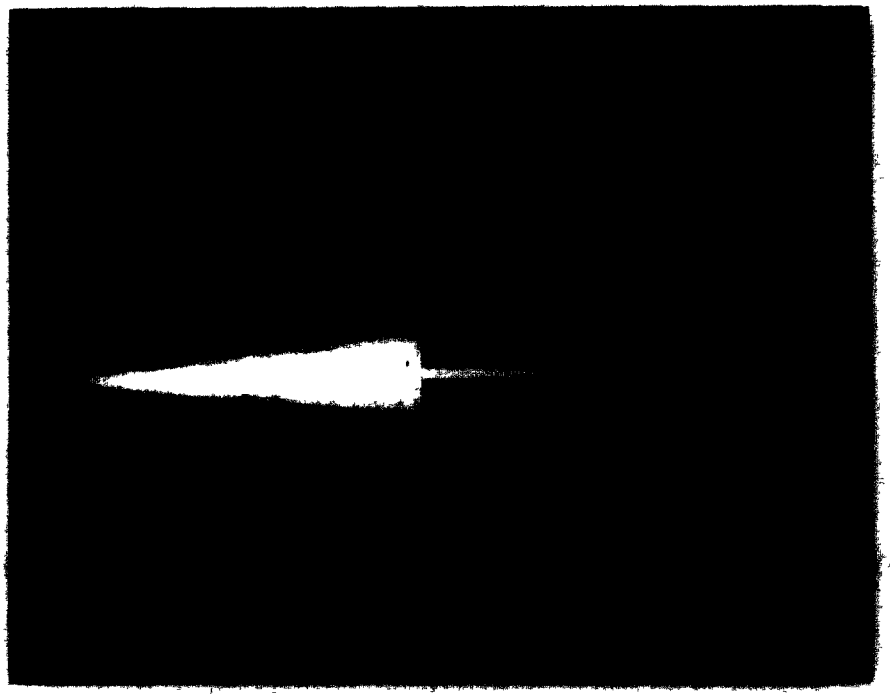

Fig. 6 Posttest photograph for the penetrator used in Test 2

Acknowledgement—The authors thank Albert J Chabai for his many helpful suggestions

REFERENCES

1. M. E. Backman and W Goldsmith, The mechanics of penetration of projectiles into targets *Int J Engng Sci* **16**, 1–99 (1978).
2. C. W. Young, Depth prediction for earth penetrating projectiles *J Soil Mech and Foundation Div. ASCE*, pp 803–817 (May 1969)
3. M. J Forrestal, D B Longcope and F R Norwood, A model to estimate forces on conical penetrators into dry porous rock. *J Appl. Mech.* **103**(1), 25–29 (1981)
4. M. J. Forrestal, F R Norwood and D. B. Longcope, Penetration into targets described by locked hydrostats and shear strength. *Int. J. Solids Structures* **17**, 915–924 (1981)
5. R. K. Byers, P Yarrington and A J Chabai, Dynamic penetration of soil by slender projectiles *Int. J Engng Sci* **16**, 835–844 (1978)
6. D. B. Longcope and D E Grady, Initial response of a rock penetrator *J Appl. Mech.* **45**(3), 559–564 (Sept 1978)
7. G R. Fowles *et al.*, Gas gun for impact studies. *Rev. of Scientific Instruments* **41**, 984–996 (1970)
8. P Yarrington, F R Norwood and D E. Grady, Comparison of experimental and computational results for reverse ballistic tests into foundry core. *SAND80-0248*, Sandia Laboratories, Albuquerque (March 1980)
9. C. B. Bailey, M. K. Gordon and R. E Jones, Brief instruction for using the Sandia numerical mathematical subroutine library on the DEC POP-10 *SLA-74-0331*, Sandia Laboratories, Albuquerque (June 1974)
10. P F. Hadala and J Q Ehrgott, Constitutive property tests on foundry core, U S Army Engineer Waterways Experimental Station, Vicksburg, MS (Nov 1977)
11. J. Q Ehrgott, Waterways experimental station, Vicksburg, MS, Letter to M. J Forrestal, Sandia National Laboratories, Albuquerque, NM (Nov. 1980)
12. J. Q Ehrgott, Development of a dynamic high pressure triaxial test device *Dynamic Rock Mechanics, Twelfth Symposium on Rock Mechanics*. Chap 10, pp 195–219 The Americal Institute of Mining, Metallurgical, and Petroleum Engineers, Inc., New York (1971)
13. J. M. Logan and J Handin, Triaxial compression testing at intermediate strain rates *Dynamic Rock Mechanics, Twelfth Symposium on Rock Mechanics* Chap. 9, pp 167–195 The Americal Institute of Mining, Metallurgical and Petroleum Engineers, Inc., New York (1971)
14. F P. Bowden and D. Tabor, *The Friction and Lubrication of Solids, Part II*, Chap. 22 Clarendon Press, Oxford (1968)
15. C S. Robinson, *The Thermodynamics of Firearms*, Chap. 16 McGraw-Hill, New York (1943)